Available online at www.sciencedirect.com
SCIENCE DIRECT®
Journal of Magnetic Resonance 164 (2003) 92–103
JMR Journal of Magnetic Resonance
www.elsevier.com/locate/jmr

Rotational resonance NMR: separation of dipolar coupling and zero quantum relaxation

Phillip R. Costa,[1] Boqin Sun,[2] and Robert G. Griffin*

Francis Bitter Magnet Laboratory, Department of Chemistry, Massachusetts Institute of Technology, Cambridge, MA 01239-4307, USA

Received 21 February 2003

Abstract

The solid state NMR technique of rotational resonance (R^2) has been used extensively to measure distances approaching 5–6 Å between ^{13}C nuclei in a variety of compounds including amyloidogenic peptides and membrane proteins. The accuracy of the distance information extracted from the time-dependent spin dynamics at R^2 is often limited by the accuracy with which the relevant zero-quantum lineshape parameters are estimated. Here we demonstrate that measurement of spinning frequency dependent magnetization exchange dynamics provides data from which both distance and zero-quantum relaxation parameters can be extracted independently. In addition to providing more accurate distance information, this technique allows examination of the zero-quantum lineshape, which can indicate the presence of correlated relaxation or chemical shift distributions between dipolar-coupled sites. With this approach we have separated the contribution of dipolar couplings and zero quantum relaxation to R^2 exchange curves. Thus, we have significantly improved the accuracy of the measurement of the intramolecular, internuclear distances between a pair of ^{13}C's in two model compounds (*N*-acetyl-D,L-valine and glycylglycine · HCl) that lie in the distance range 4.6–4.7 Å.

1. Introduction

Extracting internuclear distance information from the dipolar interactions between spin pairs has a long history in nuclear magnetic resonance (NMR). In solution spectroscopy, measuring the magnitude of the nuclear Overhauser effect between neighboring ^1H nuclei provides sufficient internuclear distance information to determine the structure of proteins and other biomolecules [1]. Experiments in solids are at a more preliminary stage, and techniques for measuring homonuclear and heteronuclear dipolar interactions are still developing rapidly. Almost all of the newer methods developed for structural studies in solids utilize the high spectral resolution provided by magic-angle spinning (MAS) [2–4] which averages anisotropic chemical shift interactions. MAS also attenuates the dipolar interactions between low-γ nuclei (e.g., $^{13}C, ^{15}N$). Because observing the effects of these interactions is often the primary goal of structural studies in the solid state, some method of reintroducing their effects—'recoupling' the relevant spin pairs [5,6]—becomes essential.

The rotational resonance (R^2) technique has been used extensively to recouple homonuclear spin pairs (particularly ^{13}C–^{13}C) in rotating solids [7,8]. Matching a multiple of the sample spinning frequency to the chemical shift difference (in Hz) between a pair of lines in the spectrum:

$$\Delta = n\nu_r, \tag{1}$$

(where Δ is the chemical shift difference, ν_r is the spinning frequency, and n is a small integer representing the order of the resonance) leads to an interference effect between the MAS-modulated spatial component of the dipolar interaction and, in the appropriate interaction frame, the chemical-shift modulated spin component of the interaction. Under these conditions MAS does not effectively attenuate the dipolar interaction and dipole-

* Corresponding author. Fax: 1-617-253-5405.
E-mail address: rgg@mit.edu (R.G. Griffin).
[1] Present address: Dean & Company, 8065 Leesburg Pike, Suite 500, Vienna, VA 22182, USA.
[2] Present address: ChevronTexaco: Exploration and Production Technology Company, 6001 Bollinger Canyon Road, San Ramon, CA 94583, USA.

1090-7807/$ - see front matter © 2003 Elsevier Inc. All rights reserved.
doi:10.1016/S1090-7807(03)00083-1

dependent effects can be observed in the spin dynamics. These include broadened resonance peaks and a much accelerated rate of longitudinal magnetization exchange. Quantification of either effect can then be used to determine the internuclear distance.

Characterization of the rate of longitudinal magnetization exchange has been the method of choice for extracting internuclear distance information with R^2 [7,9–11]. This is particularly true for weakly coupled spin pairs where spectral broadening due to the recoupled dipolar interaction may be obscured by other contributions to the linewidth (although recent work indicates that in systems with sufficiently narrow lines a transverse approach may be reasonable [12]). To observe longitudinal exchange, an initial state of difference polarization is prepared along the rotating-frame z-axis, and the time-evolution of this state is examined in a series of experiments in which the mixing period is varied over the desired range yielding what is termed a 'magnetization exchange trajectory.'

The shape of the magnetization exchange trajectory depends on a number of spin interaction parameters including the dipolar coupling constant, and the magnitude and in some cases the relative orientation of chemical shift tensors. When these are the only relevant parameters, extraction of the dipolar coupling constant (and hence the internuclear distance) becomes a single-parameter fit to the experimental data, provided that the chemical shift tensors can be appropriately characterized by other means. Under such conditions the accuracy of extracted distance information is expected to be limited primarily by the signal-to-noise ratio (S/N), and is often better than ± 0.1 Å for 4–5 Å distance measurements in model compounds.

However, magnetization exchange curves have been shown to be sensitive to at least two additional parameters, both related to the zero-quantum lineshape [11]. The *homogeneous* zero-quantum linewidth parameter, T_2^{ZQ}, characterizes the rate at which the zero-quantum coherence created during the magnetization exchange process relaxes (a Lorentzian lineshape is assumed), while the *inhomogeneous* zero-quantum lineshape characterizes the degree to which precise rotational resonance can be matched across the sample in the presence of inhomogeneously broadened single-quantum resonances. These parameters have a significant effect on the exchange dynamics when their 'magnitudes' approach that of the recoupled dipolar interaction, a condition which is usually satisfied for the weakly coupled spin pairs whose internuclear distances are of significant structural interest. In such cases the accuracy with which the zero-quantum lineshape parameters are determined often becomes the limiting factor in determining the accuracy of the R^2 distance measurement. Estimation of zero-quantum parameters from single-quantum measurements presents another alternative [8,10]. However such an approach involves assumptions about correlation between the sites which some authors have suggested lead to uncertainties in distance measurements approaching 1 Å for ^{13}C–^{13}C pairs [13].

Here we demonstrate that measurement of the resonance mismatch (e.g., spinning frequency) dependence of the longitudinal magnetization exchange process at a fixed mixing time—rather than as a function of mixing time with the spinning frequency set precisely on resonance—provides data from which dipolar coupling constants can be extracted independent of zero-quantum lineshape parameters. This is expected to yield more accurate distance information in systems in which accurate estimates of the zero-quantum lineshape parameters are unavailable. We demonstrate the process in a pair of $^{13}C_2$-labeled model compounds (*N*-acetyl-D,L-valine and glycylglycine·HCl) with intramolecular, internuclear distances on the order of 4.6–4.7 Å. Fits to the standard on-resonance, mixing time dependent experimental data show the typical strong correlation between the dipolar coupling constant and the zero-quantum linewidth. In contrast, we find that fits to the spinning frequency dependent data show very little correlation and allow separate extraction of both parameters. Such an approach can in principle also be applied to other dipolar recoupling experiments (for example heteronuclear CP [14] (under fast-spinning conditions) and homonuclear 2Q-HORROR experiments [15]).

The determination of the zero-quantum linewidth, T_2^{ZQ}, in this manner provides additional information of interest concerning the presence of correlations between the sites, which may improve significantly on estimates of zero-quantum parameters from single-quantum measurements. Our experiments indicate that such correlations between sites do not occur in the weakly coupled spin pairs examined here. More detailed zero-quantum lineshape information may also be accessible. In particular, measurement of the magnetization exchange as a function of ω_r is similar to 'CW' detection of the zero-quantum lineshape (particularly when the coupling is much smaller than the homogeneous zero-quantum linewidth). Thus, exchange curves recorded as a function of spinning frequency can provide information about the zero-quantum spectrum that goes beyond the linewidth alone.

2. Experimental methods

2.1. $^{13}C_2$-labeled samples

Synthesis and purification of $^{13}C_2$-labeled *N*-acetyl-D,L-valine (abbreviated NAV; with ^{13}C labels at the acetyl methyl and valine carboxyl carbons: $^{13}CH_3C(O)NHC(CH(CH_3)_2)^{13}CO_2H$) followed

standard methods using specifically $^{13}C_2$-labeled starting materials obtained from Cambridge Isotope Labs (Cambridge, MA) [16]. The labeled NAV was diluted 1:30 in natural abundance (calculated by comparing the integrated intensity of labeled and natural abundance resonance peaks in a series of ^{13}C CP/MAS spectra) to attenuate intermolecular dipolar interactions. Synthesis and purification of $^{13}C_2$-labeled glycylglycine·HCl (GG; with ^{13}C labels at the N-terminal α- and terminal carboxyl carbons: $NH_2{}^{13}CH_2C(O)NHCH_2{}^{13}CO_2H$) have been previously described [16] and the labeled material was diluted 1:10 in natural abundance.

2.2. NMR experiments

^{13}C NMR spectra were recorded either at 4.7 T (50 MHz ^{13}C; NAV experiments) or 9.4 T (100 MHz ^{13}C; GG experiments) using Cambridge Instruments spectrometers with data acquisition and processing software courtesy of D. Ruben. Transmission line probes were designed and constructed by C. Rienstra and B. Itin of our laboratory and utilize either 5 mm (NAV experiments) or 4 mm (GG experiments) Chemagnetics (Ft. Collins, CO) spinning modules. Spinning frequencies were controlled to within ±2 Hz of the reported values using a Doty Scientific (Columbia, SC) spinning frequency controller. Recycle delays of 3 s were used in all experiments.

The R^2 experiments were performed using the pulse sequence diagrammed in Fig. 1a. After a 2 ms cross-polarization (CP) period and an optional delay for inversion, 90° pulses are applied on the ^{13}C channel. The first $\pi/2$ pulse creates longitudinal polarization for dipolar mixing, and the second transverse polarization for detection. The time between the 90° pulses constitutes the dipolar mixing time. For time-dependent exchange curves, the sample spinning frequency was set to the isotropic chemical shift difference between the relevant spins (the center of the inhomogeneously broadened chemical shift difference distribution), and a series of experiments was performed at various mixing times spanning the desired range. At each time point, experiments with initial conditions of longitudinal sum and difference polarization were performed, the former serving as control for the latter (particularly to factor out changes in signal intensity due to probe heating effects and T_1 relaxation). We have found this to provide more reliable data than inserting a period of decoupling between longitudinal storage and selective inversion with its length adjusted to keep the overall decoupling time constant. However, there is an obvious increase in averaging time required to achieve the same spectral signal/noise. At no point did sum polarization decay by more than 5–10% as compared to the zero-mixing time intensity. Sum and difference polarization were calculated at each time point using integrated peak intensities,

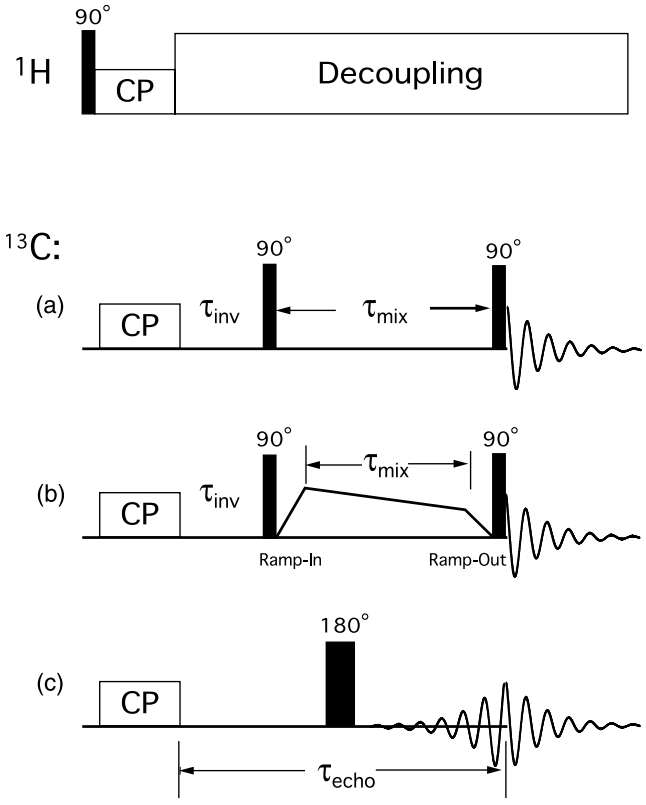

Fig. 1. Pulse sequences used in the experiments described in text. Cross-polarization (CP) and CW ^1H decoupling during subsequent dipolar mixing and signal acquisition are standard. (a) Longitudinal mixing sequence appropriate for standard rotational resonance. After CP and an optional transverse evolution period for inversion, 90° pulses transfer the polarization to the z-axis for mixing, and then to the transverse plane for detection. The time period between these pulses defines the dipolar mixing period. (b) Modified mixing sequence for rotational resonance tickling. Ramp-in and ramp-out pulses are applied just after and just prior to the initial and final pulses, respectively, to rotate the polarization to and from the near-longitudinal axis appropriate for dipolar mixing. In between these pulses the rf magnitude is ramped to pass through dipolar resonance. (c) Single π-pulse Hahn echo sequence for extracting homogeneous linewidths. The π pulse is timed to occur after an integer number of rotor periods.

and were normalized by dividing by the intensity of the zero-mixing time point in each case. The normalized difference polarization at each time point was then divided by the corresponding normalized sum polarization intensity, and subtraction of the natural abundance contribution yielded the final exchange curve.

For spinning frequency dependent exchange curves, a series of experiments was performed at spinning frequencies spanning the $n = 1$ resonance condition (typically over a range of ±0.5 kHz about $\nu_r = \Delta$). At each ω_r, four different experiments were performed: with initial conditions of sum and difference polarization and with mixing times of 0 ms and the selected longer mixing time (30 or 100 ms in the experiments described below). The 0 ms mixing time experiments at each spinning frequency allow appropriate normalization of the data

in the event of spinning frequency-dependent changes in CP transfer efficiently. These experiments could be ignored if a reliable spinning-frequency independent ^{1}H–^{13}C CP technique is employed. The final exchange curve was calculated using the normalization procedure described above.

Rotational resonance tickling (R^2T) [17] was used to verify the effective internuclear distance in NAV. R^2T, in comparison with conventional R^2 experiments, improves spectral resolution because it is off R^2. Further, it reduces the dependence of the dipolar-driven magnetization exchange on the zero-quantum parameters. These improvements results from the utilization of a small (quasi-adiabatic) ramped rf field at the beginning and end of the mixing period. In the presence of a small rf field during the mixing period, the difference of the effective fields at the coupled spins drives the polarization transfer. When the rf amplitude ramps slowly through the R^2 resonance condition in the rotating frame, transfer of polarization between the spins of interest occurs adiabatically. The pulse sequence is similar to that for standard R^2, however a variable amplitude rf is applied between the 90° pulses to sweep the system through dipolar resonance (Fig. 1b). Immediately after the first 90° pulse creates longitudinal polarization, a 'ramp-in' is used to quasi-adiabatically prepare the spins for the mixing period, τ_{mix}. Following the mixing period, a ''ramp-out'' pulse preceding the final 90° pulse reverses the process. These pulses each typically last 200–300 μs. In between, the rf magnitude is ramped over a fixed range (from one side of the dipolar resonance to the other, typically of the order of a few kilohertz), with the duration of this ramp determining the overall mixing time. Magnetization exchange as a function of rf ramp rate is measured by repeating the basic experiment for a series of different mixing times. Again, both the sum and difference polarization are prepared as initial states, and the final normalized curve is calculated as described above.

Single π pulse Hahn echo experiments [18] with transverse evolution during the echo period, were used to measure the homogeneous linewidth of each ^{13}C labeled site (Fig. 1c). Spinning frequencies were set well away (at least 0.7 kHz) from R^2 conditions to eliminate dipolar contributions to the signal decay, and the echo mixing period was timed so that the center of the π pulse occurred at an integer number of rotor periods after the end of CP.

2.3. Numerical simulation of spin dynamics

Exchange curves were calculated using the method initially described by Levitt et al. [8], with modifications where necessary to include a weighted distribution of isotropic chemical shift differences. The details of the R^2T exchange curve calculations are discussed elsewhere [17]. The CSA parameters necessary for the calculations included the magnitude of the principal components, but not the relative tensor orientation. These values were extracted from the sideband patterns in slow-spinning spectra and were in agreement with previously published values.

In what follows differences between exchange curves are characterized as ''average square deviations.'' For time-dependent curves this is calculated according to:

$$\sigma^2 = \frac{1}{N}\sum_{n=1}^{N}\left[x^{(1)}(t_n) - x^{(2)}(t_n)\right]^2, \tag{2}$$

where N is the number of points along the curves at which the calculation is made, the superscripts (1) and (2) denote the two curves being compared, and $x^{(i)}(t_n)$ represents the value of the nth time point along the ith curve. Spinning frequency-dependent curve comparisons are calculated analogously.

3. Background

3.1. Longitudinal magnetization exchange—time-dependent spin dynamics

The spin dynamics at rotational resonance have been described in detail by several authors [7,8,19]. Here we focus on the features relevant to longitudinal magnetization exchange. For a dipolar-coupled, homonuclear two-spin system, matching the spinning frequency precisely to the difference in isotropic chemical shifts yields a purely dipolar average Hamiltonian (in the appropriate interaction frame). This Hamiltonian couples the central two levels of the typical two spin-1/2 energy level diagram—it has zero-quantum character—and can be represented as a transverse vector in the fictitious spin-1/2 subspace [20,21] corresponding to the coupled pair of energy levels. Longitudinal difference polarization corresponds to a longitudinal vector in this space. Further, the coherent evolution of a 2-spin system precisely at R^2 consists solely of a rotation of the initial longitudinal state vector about the transverse Hamiltonian vector, between states of difference polarization and zero-quantum coherence. According to this description, detection of difference polarization during the magnetization exchange process in a single crystallite would yield an cosinusoidal oscillation described by:

$$\langle I_z - S_z\rangle(t) = \cos\left(|\varpi_B|t\right) \tag{3}$$

($|\varpi_B|$ is the magnitude of the recoupled dipolar interaction). Powder averaging over the range of recoupled dipolar interaction strengths in a polycrystalline sample then yields a characteristic damped oscillation.

Relaxation modifies the coherent dynamics in a manner that depends on its rate relative to the magnitude of the recoupled interaction [22]. Relaxation is

anisotropic in the fictitious spin-1/2 space—longitudinal components of the state vector relax according to T_1 while transverse components relax according to T_2^{ZQ}. In many samples T_1 is sufficiently long that it can be ignored, and we can focus solely on the relaxation of zero-quantum coherence (transverse vectors in the fictitious spin space) described by T_2^{ZQ}. If the recoupled interaction is sufficiently large to induce several 360° rotations of the state vector on a timescale short compared to T_2^{ZQ}, then the observed dynamics are simply an exponentially damped version of the ideal coherent dynamics. This is as if relaxation were isotropic and governed by an overall time constant twice the zero-quantum value. Simple exponential damping of the ideal coherent dynamics does not occur in systems in which zero-quantum relaxation has a significant effect on the timescale of a single coherent oscillation. Levitt et al. [22], have calculated the modified dynamics under these conditions:

$$\langle I_z - S_z\rangle(t) \cong \mathrm{e}^{-t/2T_2^{ZQ}}\left[\cosh(Rt/2) + \frac{r}{R}\sin(Rt/2)\right], \qquad (4)$$

when $R^2 > 0$ (where $R = [(T_2^{ZQ})^{-2} - 4|\varpi_B|^2]$, $r = (T_2^{ZQ})^{-1}$). As relaxation begins to dominate (the 'fast relaxation' regime: $R^2 \gg 0$), oscillations in the observed dynamics disappear, and the decay of difference polarization as a function of time approaches an exponential function with a time constant proportional to $(T_2^{ZQ}|\varpi_B|^2)$. Specifically:

$$\langle I_z - S_z\rangle(t) \cong \mathrm{e}^{-t(T_2^{ZQ}|\varpi_B|^2)} = \mathrm{e}^{-t/T_{\mathrm{exchange}}}. \qquad (5)$$

Thus, compensating changes in the coupling constant and the rate of zero-quantum relaxation can lead to exchange curves with identical T_{exchange} values, particularly in the fast-relaxation limit. In this regime extracting accurate distance information from experimental data obtained under these conditions requires an accurate estimate of T_2^{ZQ}. This situation is illustrated in Fig. 2a, where we show the simulated decay of difference polarization as a function of time for a dipolar-coupled spin pair with an internuclear distance of 4.7 Å (corresponding to a dipolar coupling constant $b_{IS} = 73$ Hz), and a $T_2^{ZQ} = 1.4$ ms. These parameters, and the chemical shift parameters used in the simulations, are typical values for the NAV experiments described below. In Fig. 2b we show a contour plot of the average square deviation between the curve in Fig. 2a and a series of simulations generated using a range of dipolar coupling constant and zero-quantum relaxation values. The minimum that extends from the lower left to the upper right corner of the 2D plot indicates that the curve in Fig. 2a can be closely approximated by simulations using a range of dipolar coupling values, as long as T_2^{ZQ} is decreased appropriately to account for increases in the dipolar coupling constant (and vice-versa). The point is further emphasized by superimposing in Fig. 2a two additional simulations calculated assuming internuclear

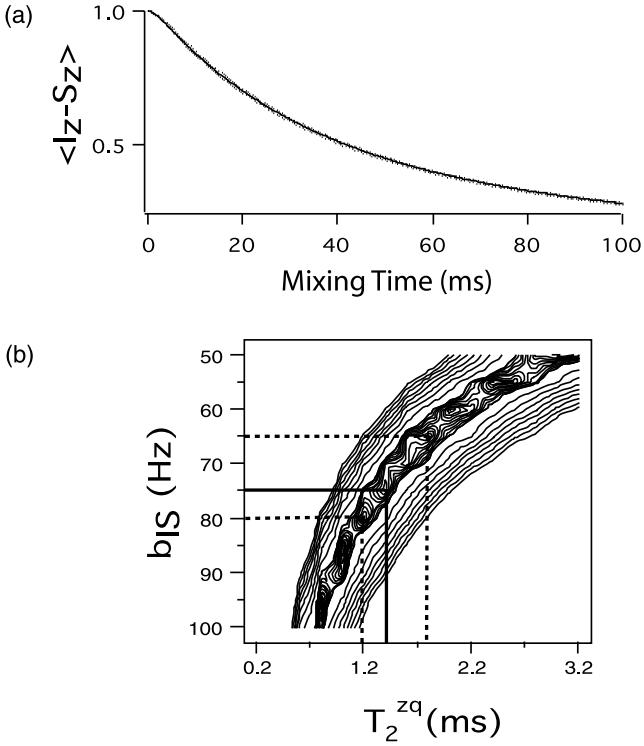

Fig. 2. (a) Simulated time-dependent magnetization exchange curve for a spin pair with $b_{IS} = 73$ Hz and $T_2^{ZQ} = 1.4$ ms (solid line). Superimposed on this line are two additional dotted lines which are not distinguishable from the solid curve. They correspond to b_{IS} of 65 and 80 Hz and T_2^{ZQ} of 1.8 and 1.2 ms, respectively. (b) 2D contour plot comparison of a series of simulations at a range of coupling constants and T_2^{ZQ} values to the curve in (a). The plotted value is the 'average square deviation.' The contour levels in this and subsequent 2D plots vary from 10^{-2} to 10^{-3} in increments of 10^{-3}, and then from 10^{-3} to 10^{-4} in increments of 10^{-4} (this corresponds to root-mean-square (rms) deviations plotted from 1% to 10%). The vertical and horizontal lines in (b) indicate b_{IS} and T_2^{ZQ} values for simulations in (a).

distances of 4.85 and 4.55 Å ($b_{IS} = 65$ and 80 Hz) and with the T_2^{ZQ} values (1.8 and 1.2 ms, respectively) which provide the best match to the original 4.7 Å curve. As can be surmised from the figure, these curves are not distinguishable from one another. The similarity among the three simulations illustrates the difficulty of extracting unambiguous distance information from R^2 exchange curves when the zero-quantum relaxation rate is not known.

3.2. Mismatch-dependent spin dynamics

An alternative to measuring R^2 exchange dynamics as a function of mixing time, τ_{mix}, is measurements as a function of resonance mismatch, $(\Delta - \nu_r)$ at a fixed mixing time. The motivation for such a measurement is illustrated in Fig. 3. Calculation of the mismatch-dependence of exchange for a 2-spin system with a 4.7 Å internuclear distance and T_2^{ZQ} values of either 1 ms or 4 ms (other simulation parameters appropriate for

NAV) after 100 ms of mixing are diagrammed in Fig. 3a. Note that the labels along the vertical axis run opposite to the normal sense to yield a rotational resonance 'peak' rather than a 'trough.' We display only one-half of the resonance because the symmetry of the effect ensures that both halves are essentially identical (particularly if we ignore the small, Bloch–Siegert-like shifts in the resonance condition [22], and any asymmetric distribution in chemical shift differences). With $T_2^{ZQ} = 4$ ms, there is less exchange observed off-resonance and more exchange on-resonance, as compared to the curve calculated using $T_2^{ZQ} = 1$ ms. These curves demonstrate that increases in T_2^{ZQ} narrow the width and increase the intensity of the observed resonance condition (as indicated by the arrows in the figure), leaving the overall area under the resonance relatively unchanged. In contrast, Fig. 3b demonstrates that increases in the dipolar coupling constant both broaden the width and increase the intensity of the resonance as indicated by the arrows (calculations assume $T_2^{ZQ} = 2$ ms and internuclear distances of approximately 5.3 and 4.2 Å, corresponding to b_{IS} of 50 and 100 Hz).

The qualitatively different response of the resonance shape to changes in the two parameters suggests that they may be extracted separately from experimental data without strong correlations. This idea is further supported by Fig. 4 where the solid line in Fig. 4a shows the ω_r dependent exchange curve expected for the 4.7 Å ($b_{IS} = 73$ Hz, $T_2^{ZQ} = 1.4$ ms) parameter set used in Fig. 2. The 2D contour plot in Fig. 2b shows the average square deviation over a range of coupling constants and zero-quantum relaxation rates. The shape of the 2D plot indicates that both the coupling constant and T_2^{ZQ} can, at least in principle, be extracted independently of one another with some accuracy. The additional simulations in Fig. 4a (dotted and dashed lines) show the best fits with coupling constants corresponding to distances of 4.55 and 4.85 Å for comparison to Fig. 2a.

3.3. The effects of chemical shift dispersion

A distribution of isotropic chemical shifts at each of the recoupled sites (termed chemical shift dispersion, or CSD) can further modify the coherent rotational resonance dynamics since precise matching of the resonance condition for all spin pairs in the sample may no longer be possible. With the spinning frequency placed at the center of the resulting isotropic chemical shift difference distribution one generally maximizes resonance match. However, those spin pairs whose shift difference lies away from the center of the distribution will evolve under a recoupled Hamiltonian with a longitudinal component (in the fictitious spin space). The degree to which this affects the dynamics depends upon the rela-

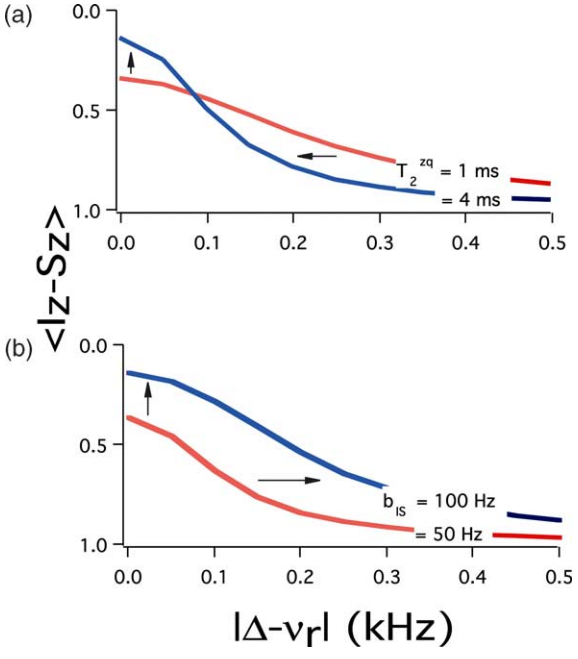

Fig. 3. Variation in magnetization exchange curves collected as a function of absolute resonance mismatch due to changes in (a) T_2^{ZQ} (1 and 4 ms, with $b_{IS} = 73$ Hz) and (b) b_{IS} (50 and 100 Hz, with $T_2^{ZQ} = 2$ ms. Note that the labels along the vertical axis run opposite to the normal sense to yield a rotational resonance 'peak' rather than 'trough.' Only one-half of the resonance is displayed because the symmetry of the effect ensures that both halves are essentially identical.

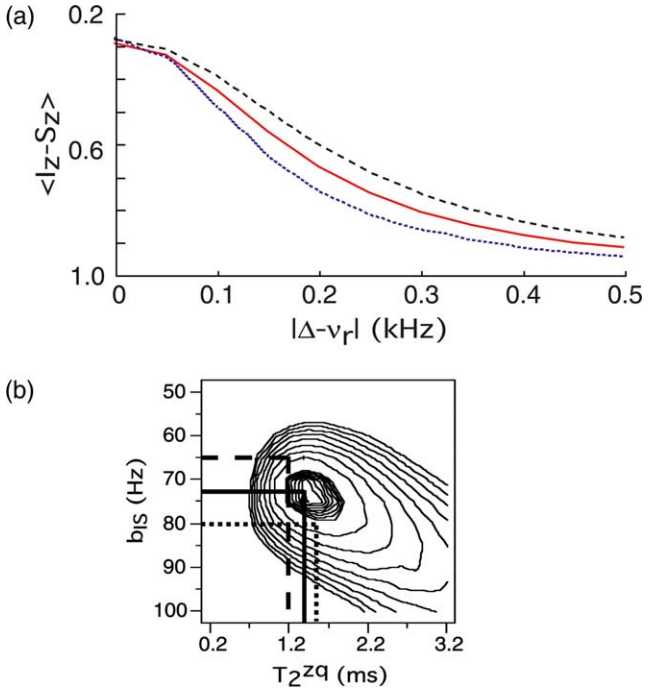

Fig. 4. (a) Resonance mismatch-dependent exchange curve with parameters from Fig. 2a (solid line). (b) 2D 'average square deviation' contour plot. Vertical and horizontal lines indicate b_{IS} and T_2^{ZQ} values for additional simulations in (a) (dotted lines).

tive sizes of the resonance mismatch, $\Delta - \nu_r$ and the recoupled dipolar components of the Hamiltonian. When the magnitude of the latter approaches or exceeds the former (and hence significantly affects the orientation and magnitude of the recoupled interaction) we expect significant CSD-dependent effects.

We can view the difference distribution as the inhomogeneous component of the zero-quantum lineshape, with T_2^{ZQ} representing the linewidth of the homogeneous component (a Lorentzian shape is assumed). Both of these effects act to damp the coherent, oscillatory time-dependent dynamics. Particularly when the recoupled interaction is comparable to or larger than the zero quantum relaxation rate, $(T_2^{ZQ})^{-1}$ (i.e., when significant zero-quantum coherence is created during the exchange process), they have qualitatively different effects that must be distinguished to accurately simulate the spin dynamics. Transverse echo experiments allow separation of inhomogeneous and homogeneous contributions to the lineshape of the relevant single-quantum coherences, and estimating the homogeneous zero-quantum linewidth as the sum of the homogeneous single-quantum linewidths has been described [11,23]. Calculation of the inhomogeneous zero-quantum lineshape from the inhomogeneous components of the single-quantum lineshapes is also straightforward using the appropriate convolution (see below). In both of these calculations, however, one assumes that the underlying effects giving rise to the single-quantum behavior is uncorrelated at the two sites. For instance, the 'random local fields' that lead to homogeneous dephasing of single-quantum coherence will also dephase zero-quantum coherence only to the extent that the local fields at the two sites are different [23]. Similarly, slight structural variations that lead to variations in chemical shift at one site [24] must not imply specific structural variations at the second site which would lead to correlation in their chemical shift distributions.

The need for distinguishing between the effects of inhomogeneous and homogeneous zero-quantum lineshape components has been clearly demonstrated by 'control' experiments in $^{13}C_2$-labeled amyloid peptides with large inhomogeneous linewidths (1–3 ppm) [10,11,13]. With the labeled sites separated by two bonds (i.e., carbonyl and α-carbon labels on successive residues), the internuclear distance is approximately fixed by molecular geometry and yields a relatively large coupling constant ($b_{IS} \sim 0.5$ kHz). Under typical experimental conditions, this coupling is strong enough to drive coherent, time-dependent oscillations while not being so large as to essentially eliminate zero-quantum damping effects. By close examination of the time-dependent dynamics in these cases, various authors have proposed to detect evidence of correlation in both homogeneous and inhomogeneous single-quantum parameters as just described [13]. Proposals have been made to extrapolate zero-quantum parameters measured in these systems to the more weakly coupled spin pairs whose internuclear distances are of structural interest, and where the small size of the coupling makes it difficult to use similar techniques to extract zero-quantum lineshapes information. One clear problem with this approach is the expected distance-dependence of correlation, which may make extrapolation of zero-quantum parameters from strongly coupled spins to more weakly coupled spins suspect. The techniques that we present here represent a reliable alternative for extracting distance information without resorting to such measures.

3.4. The fast relaxation regime

Extracting the dipolar coupling constant and zero-quantum relaxation rate from mismatched-dependent R^2 exchange curves is complicated by the additional dependence of the observed dynamics on chemical shift dispersion. Because the damping effects of the two components of the zero-quantum lineshape (homogeneous characterized by T_2^{ZQ}, and inhomogeneous characterized by both a linewidth and shape) differ considerably under certain conditions, their effects generally must be included separately in the simulations with which distance information is extracted from experimental data. In these cases the measured R^2 linewidth provides a constraint on a qualitative 'sum' of the widths of the two ZQ lineshape components (given a certain value for the coupling constant), so that only the relative amounts of the two contributions to the dynamics remain unknown. Furthermore, increases in one ZQ linewidth component (homogeneous or inhomogeneous) at least partially compensates for decreases in the other. Therefore, simulations with a fixed coupling constant and overall zero-quantum linewidth, but with varying division into inhomogeneous and homogeneous components, are often very similar. Measurement of the R^2 width at a series of mixing times can facilitate separation of the two lineshape parameters because the time dependence of their contribution to the dynamics differs significantly. Exploiting these effects reduces the uncertainty in extracting distance information from R^2 data when ZQ lineshape components are not known accurately by other means.

Nevertheless, we can avoid the need to separately include homogeneous and inhomogeneous ZQ components in simulations if we perform experiments under conditions in which their damping effects are similar. This occurs in the 'fast-relaxation' regime: when the zero-quantum relaxation rate (i.e., $(T_2^{ZQ})^{-1}$) dominates the rate of zero-quantum coherence creation (determined by the magnitude of the recoupled dipolar interactions). The effect is illustrated in Fig. 5, where simulations with fixed coupling constant ($b_{IS} = 60$ Hz) and zero-quantum linewidth (~350 Hz, corresponding

to an effective T_2^{ZQ} of 3.1 ms), but with varied division of the ZQ lineshape into homogeneous and inhomogeneous components, are compared. The near identity of the simulations demonstrates that separating the two components is unimportant under these conditions. This holds equally well for spinning frequency dependent R^2 data (representative simulations not shown). (Note that at very long mixing times the difference between the two components can again become important.)

We can enter the 'fast-relaxation' regime by lowering the ^{1}H decoupling power enough to sufficiently decrease the value of T_2^{ZQ}. Measuring homogeneous linewidths provides one indicator of the degree to which the fast-relaxation condition is satisfied, and in typical experiments strict fulfillment of the condition is not required. In the fast-relaxation regime, we fit R^2 data solely using b_{IS} and T_2^{ZQ} parameters. The homogeneous ZQ linewidth will be an 'effective'parameter one that includes whatever inhomogeneous contribution is present. Although the inhomogeneous ZQ component may have a non-Lorentzian shape, the assumption of an overall Lorentzian ZQ lineshape implicit in the effective T_2^{ZQ} is an adequate approximation, at least for the experimental data we show below.

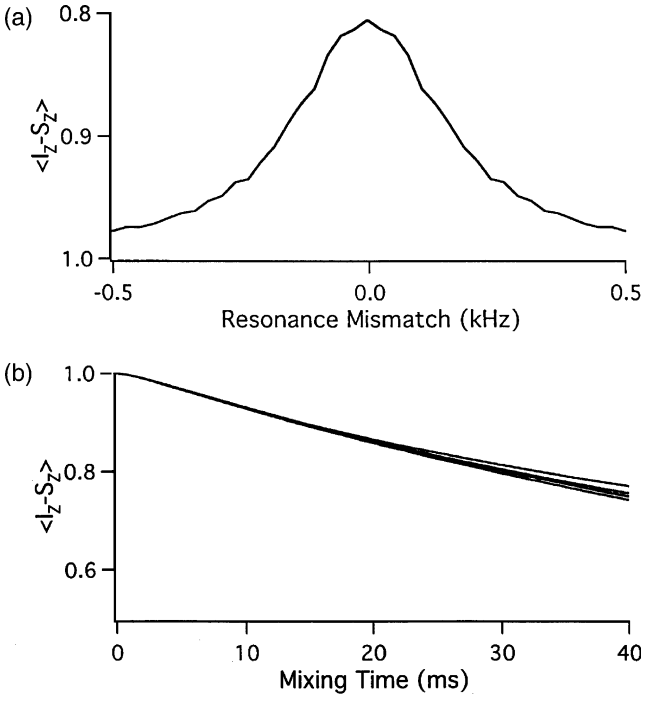

Fig. 5. Calculated exchange curves for $b_{IS} = 60$ Hz and a fixed zero quantum (ZQ) linewidth of 0.32 kHz. (a) Spinning frequency dependent exchange curve with 30 ms of mixing assuming a purely homogeneous ZQ line (the width of the observed R^2 resonance is slightly larger than the true ZQ linewidth). (b) Five time-dependent exchange curves calculated assuming homogeneous (T_2^{ZQ}, in ms) and inhomogeneous (shape assumed Lorentzian, in kHz) ZQ components as follows: 3.1 ms/0.0 kHz, 3.7/0.05, 4.5/0.10, 5.93/0.15, 8.5/0.20 (all pairs add to the same overall ZQ linewidth).

In two spin systems with little or no inhomogeneous ZQ linewidth, a loss of polarization transfer efficiency is expected with the decreased T_2^{ZQ} values associated with the fast-relaxation regime. In systems with significant inhomogeneous broadening, however, the increased width of the resonance condition in the fast-relaxation regime compensates for the decreased on-resonance exchange rate (faster exchange in the off-resonance part). The result is often a minimal decrease, and in some cases a measurable increase, in the dipole-driven polarization transfer rate at R^2 in inhomogeneously broadened samples.

4. Results and discussion

4.1. Longitudinal exchange dynamics in $^{13}C_2$-NAV

Analysis of MAS spectra of the $^{13}C_2$-labeled *N*-acetyl-D,L-valine sample (labels at the acetyl methyl and valine carboxyl carbons), obtained at 4.7 T, yield the following chemical shift parameters: isotropic chemical shift difference $\Delta = 7.518$ kHz; methyl CSA $\delta = 1.25$ kHz, $\eta = 0.5$; carboxyl CSA $\delta = -3.75$ kHz, $\eta = 0.56$. The molecular structure of the compound determined by X-ray crystallography [25] indicates an intramolecular, internuclear distance of 4.67 Å, corresponding to a dipolar coupling constant of 75 Hz. Rotational resonance tickling (R^2T) experiments were performed to verify the magnitude of the dipolar coupling. Spinning at $\omega_r/2\pi = 8.3$ kHz required application of a 1.7 kHz rf field, carrier frequency precisely between the lines, to induce dipolar resonance, confirmed by measurement of the dipolar resonance condition shown in the inset of Fig. 6. Ramping through the dipolar resonance (the ramp range is indicated by the bar under the inset resonance condition) at series of ramp rates yielded the exchange curves shown in the larger figure (filled symbols). Data was acquired at several ^{1}H CW decoupling field strengths (circles, 105 kHz; squares, 80 kHz; triangles, 50 kHz) to verify the absence of decoupling-power dependence. Comparison to simulated curves (calculated assuming a 50 Hz 2-quantum relaxation rate) indicates a coupling constant between 70 and 75 Hz, very close to that calculated from the X-ray structure. Note that the high dilution level (1:30) drastically attenuated any intermolecular effects that might otherwise have been present.

Fig. 7a shows the time-dependent $n = 1R^2$ exchange curve ($\omega_r/2\pi = 8.7518$ kHz) obtained from NAV at high ^{1}H decoupling power (110 kHz; filled circles). The presence of substantial oscillations implies a zero-quantum relaxation rate that does not dominate the magnitude of the recoupled dipolar interaction. This is confirmed by single π-pulse Hahn echo experiments that yield single-quantum homogeneous linewidths of 7 and

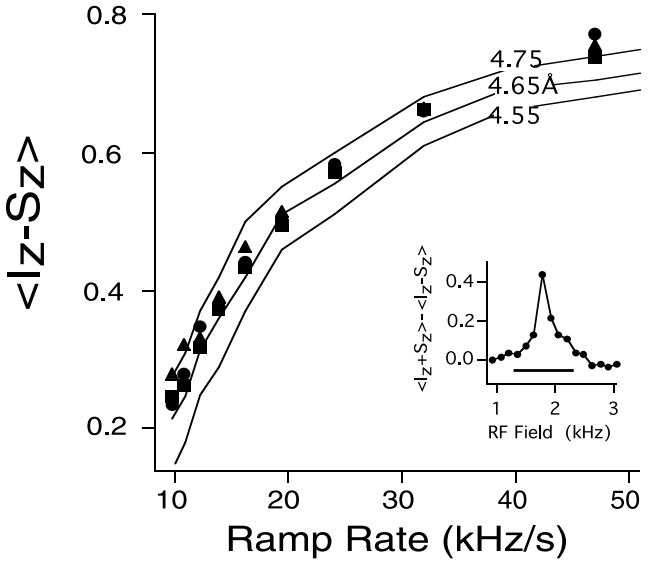

Fig. 6. Rotational resonance tickling (R^2T) applied to $^{13}C_2$-labeled NAV. The inset shows the dipolar resonance (exchange as a function of rf field strength at a fixed mixing time, in this case 100 ms), with a line underneath indicating the rf ramp range for the ramped R^2T experiment. The larger plot shows the decay of normalized difference polarization as a function of ramp rate (circles, 110 kHz ^{1}H decoupling during mixing; squares, 80 kHz; triangles, 50 kHz). Comparison to the simulated curves (calculated using a 50 Hz 2-quantum relaxation rate) indicates a coupling constant between 70 and 75 Hz, which compares favorably with the 75 Hz coupling (corresponding to a 4.67 Å distance) calculated from the X-ray crystal structure. Note that the solid lines denoting the simulated curves connect a finite number of calculated values; this explains the 'kinked' appearance of these lines.

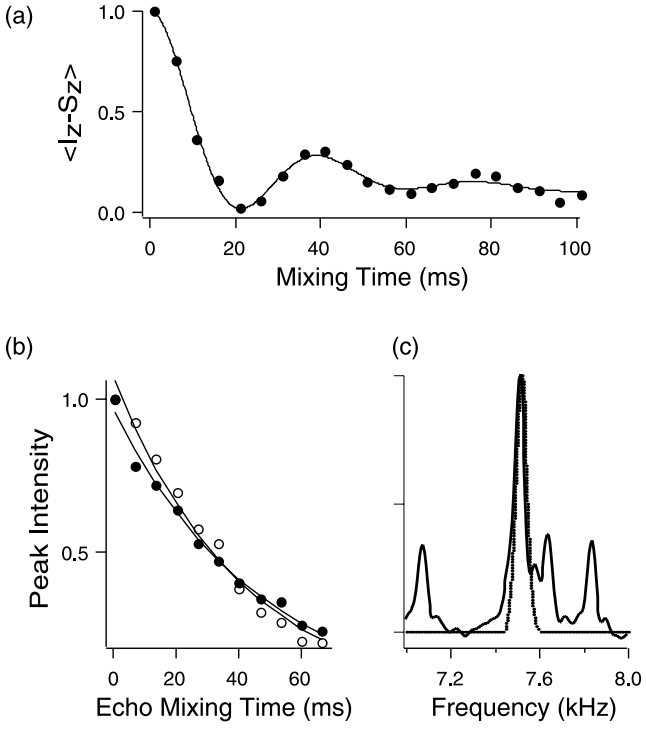

Fig. 7. Longitudinal magnetization exchange at the $n = 1$ rotational resonance for $^{13}C_2$-labeled NAV. (a) Longitudinal exchange curve at the $n = 1$ resonance ($\omega_r/2\pi = 7.518$ kHz) with 105 kHz ^{1}H decoupling field strength. Simulation (solid line) requires inclusion of relaxation ($T_2^{ZQ} = 22$ ms) and chemical shift difference distribution effects (the latter reduced from 60 to 40 Hz (Gaussian) to correct for magnet inhomogeneity). (b) The decay of ^{13}C methylene (open circles) and carboxyl (closed circles) polarization as a function of transverse evolution time in a standard single π-pulse Hahn echo experiment. Exponential fitting yields homogeneous linewidths of 7 and 8 Hz, respectively. (b) Convolution of the methylene resonance with the mirror image of the carboxyl resonance yields the expected 'chemical shift difference distribution' (hence calculated by multiplying the FID by a copy of itself with the imaginary component inverted, followed by negative exponential multiplication by 15 Hz to remove homogeneous broadening, followed by FT). A 60 Hz Gaussian (dotted line) roughly fits the experimental peak. (Data in (b) and (c) acquired at $\omega_r/2\pi = 8.2$ kHz and with 105 kHz ^{1}H decoupling.)

8 Hz for the methyl and carboxyl carbons, respectively (Fig. 7b). Simulations based on the chemical shift parameters given above, a dipolar coupling constant of 72.5 Hz, and including the T_2^{ZQ} value calculated from the single-quantum echo measurements (22 ms), do not, however, match the experimental data. A correction is required for the distribution of chemical shifts at each site. If we assume that the inhomogeneous distributions at the two sites are not correlated, then we can easily calculate the expected difference distribution (for instance, (complex) multiplication of the FID by a copy of itself with the imaginary part inverted, and with appropriate negative line-broadening before Fourier transformation to remove the homogeneous component of the linewidth). For the NAV sample the spectrum resulting from this process is illustrated in Fig. 7c. A 60 Hz Gaussian roughly fits the relevant peak (the others derive from natural abundance background signals). Because some fraction of the single-quantum linewidth derives from magnet inhomogeneity, and hence is expected to correlate between the sites in a single molecule, the contribution of that fraction must be subtracted from the measured difference distribution to yield the width of the actual distribution. In this case the width of the difference distribution was reduced to 40 Hz, and the resulting simulation (solid line) closely matches the experimental data. The closeness of the fit in this case provides at least circumstantial evidence that the 'no-correlation' assumption used to calculate zero-quantum parameters from single-quantum measurements is acceptable.

Nevertheless, measuring the exchange dynamics as function of resonance mismatch provides a means of extracting the coupling constant directly from R^2-induced dynamics without resorting to estimates of the zero-quantum parameters. Reducing the decoupling power to 40 kHz allows us to enter the 'fast-relaxation' regime defined above, and yields the exchange curve as a function of spinning frequency shown in Fig. 8a, where the mixing time was set to 100 ms. The measured curve as a function of spinning frequency (inset of Fig. 8a) on

both sides of the resonance condition (i.e., with positive and negative mismatch values) was averaged about the central value to yield the experimental data points. These are shown as a function of absolute mismatch in the larger plot (an asymmetric inhomogeneous ZQ lineshape contribution will be averaged by this process, simplifying the fitting process). Comparison of this experimental data to a series of simulated curves using dipolar coupling constants and zero-quantum relaxation rates spanning the expected ranges yields the 2D contour plot shown in Fig. 8b. The best fit is obtained with a coupling constant of 72.5 ± 3 Hz and a T_2^{ZQ} value of 1.4 ± 0.1 ms, both values extracted independently of one another. Simulated curves superimposed on the experimental data in Fig. 8a show the best-fit curve (solid line) and, for comparison, curves calculated assuming 65 and 80 Hz coupling constants (dotted lines) with the appropriate zero-quantum values to maximize the fit (1.5 and 1.4 ms, respectively).

The conventional time-dependent R^2 exchange curve (obtained at the same decoupling field strength—40 kHz) is shown in Fig. 8c for comparison, with the associated 2D contour plot in Fig. 8d. The contour plot shows the characteristic correlation between the dipolar coupling constant and T_2^{ZQ}, which precludes extraction of the former without knowledge of the latter. In this case, echo measurements yield a 3.0 ms value for T_2^{ZQ}, suggesting a coupling constant on the order of 62 Hz. Calculation of an effective T_2^{ZQ} directly from the observed linewidths, to include the inhomogeneous contribution to the zero-quantum linewidth, yields a value of 2.29 ms, which then yields a dipolar coupling constant (71 Hz) which closely approximates the correct value. This is further evidence that the assumptions inherent in estimating zero-quantum parameters from single-quantum measurements are valid, at least in this sample. The discrepancy between the zero-quantum linewidth values estimated from the single-quantum linewidths (2.3 ms) and fitting of the spinning frequency dependent exchange curve (1.4 ms) is likely related to the presence of slow- and fast-relaxation components.

4.2. Longitudinal exchange dynamics in $^{13}C_2$-GG·HCl

Identical experiments were performed in $^{13}C_2$-labeled glycylglycine·HCl (GG). The chemical shift parameters extracted from MAS spectra at 9.4 T were: $\Delta = 12.891$ kHz; α-carbon CSA $\delta = 1.99$ kHz, $\eta = 0.99$; carboxyl carbon $\delta = -9.08$ kHz, $\eta = 0.47$. The internuclear distance calculated from the neutron diffraction structure [26] is 4.56 Å, corresponding to a dipolar coupling constant of 80 Hz. Previous experiments performed on the 1:10 diluted sample used here, including a detailed

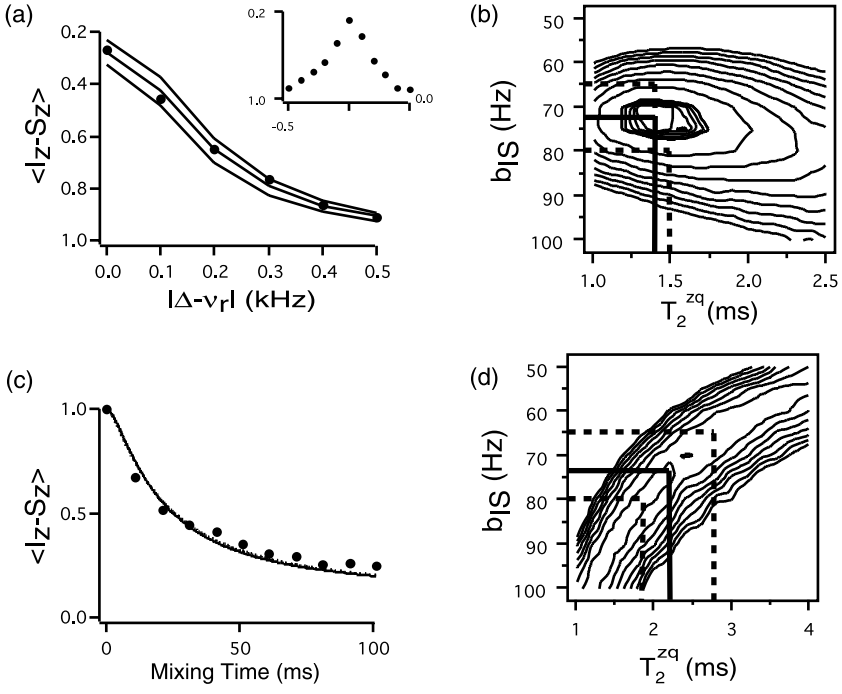

Fig. 8. Magnetization exchange as a function of resonance offset near the $n = 1$ rotational resonance for $^{13}C_2$-labeled NAV. (a) The decay of difference polarization as a function of absolute resonance mismatch (the inset shows the result without symmetrization) with a decoupling power of 40 kHz and mixing time of 100 ms. (b) Comparison of a series of simulations at a range of coupling constants and T_2^{ZQ} values to the experimental data in (a) (plotted values correspond to 'average square deviations'). Vertical and horizontal lines indicate values for corresponding simulations in (a). (c–d) identical to (a–b), except that data (decay of difference polarization) collected as a function of time, with spinning frequency set on-resonance ($\omega_r/2\pi = 7.518$ kHz).

series of RFDR experiments [27]. In what follows we will assume that this is the correct value.

Fig. 9 illustrates the experimental data and fitting results for this sample in an analogous manner to what is presented in Fig. 8 for NAV. The data were collected at a ^{1}H decoupling field strength of 80 kHz, and the spinning frequency dependent exchange measurements were made with a 30 ms mixing time. The 2D contour plot showing the fit to the spinning frequency-dependent data (Fig. 9b) clearly indicates a coupling constant of 95 ± 1.5 Hz independent of T_2^{ZQ}, and suggests a value for the latter of 1.25 ± 0.1 ms. The time-dependent data shows the typical correlation between b_{IS} and T_2^{ZQ}; with the effective T_2^{ZQ} value calculated from the observed linewidths (1.29 ms), the correct dipolar coupling constant is extracted. Again, the estimation of zero-quantum parameters from single-quantum measurements is acceptable. Furthermore, the value for T_2^{ZQ} extracted from fitting the spinning frequency-dependent exchange curve data agrees with that calculated directly from the single-quantum linewidths. That all of the measurements are internally consistent adds additional support to the conclusions drawn from the data.

4.3. Resonance mismatch measurements in related resonance techniques

There exists a series of resonance recoupling experiments with strong similarities to R^2. These include heteronuclear CP [14] (under fast-spinning conditions) and homonuclear 2Q-HORROR experiments [15]. In both cases rf is applied to create a match between the sum or difference of the effective field strengths of the relevant spin pair and some (low) integer multiple of the spinning frequency. Time-dependent, on-resonance magnetization exchange dynamics in these experiments are expected to be damped by effects including rf inhomogeneity and relaxation of the relevant (either zero or double) multiple-quantum coherence, making it difficult to extract accurate distance information from time-dependent exchange data. Mismatch-dependent exchange data, i.e., at a fixed mixing time and as a function of either rf field strength or spinning frequency (e.g., a CP Hartmann–Hahn matching spectrum [28]), provides the same type of complementary information for these experiments that the spinning frequency-dependent data we have described here provides for R^2 experiments. Rf-inhomogeneity and related time-dependent damping influences will manifest themselves as broadening in the mismatch spectrum, and combined analysis of mismatch-dependent and on-resonance, time-dependent exchange curves should allow extraction of more accurate distance information. Under the appropriate ^{1}H decoupling conditions (i.e., the fast-relaxation regime), fitting of mismatch-dependent data alone should allow extraction of distance information in these experiments, as we have shown here for R^2.

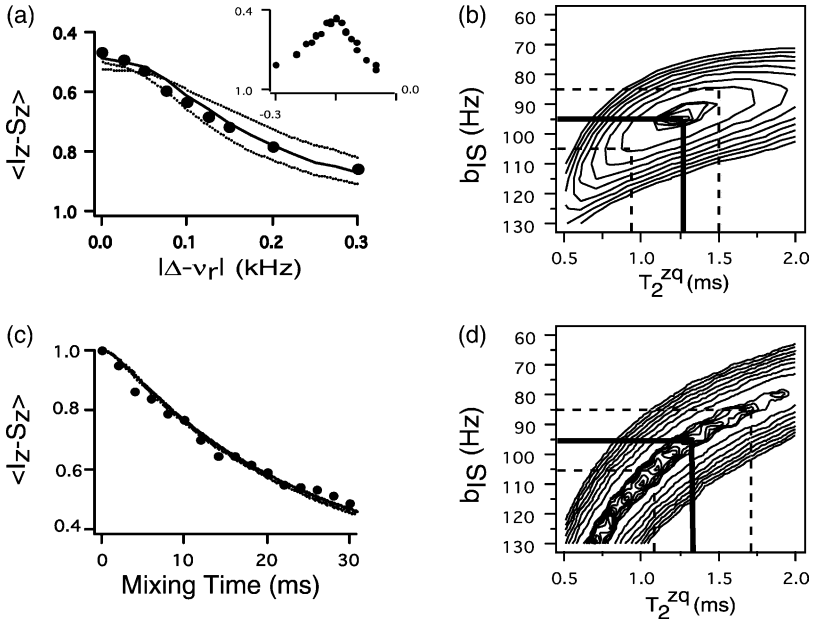

Fig. 9. Magnetization exchange as a function of resonance offset near the $n = 1$ rotational resonance for $^{13}C_2$-labeled GG·HCl. (a) The decay of difference polarization as a function of absolute resonance mismatch (inset shows result without symmetrization) with a decoupling power of 80 kHz and a mixing time of 30 ms. (b) Comparison of a series of simulations at a range of coupling constants and T_2^{ZQ} values to the experimental data in (a) (plotted values correspond to 'average square deviations'). Vertical and horizontal lines indicate values for corresponding simulations in (a). (c–d) identical to (a–b), except that data (decay of difference polarization) were collected as a function of time, with the spinning frequency set on-resonance ($\omega_r/2\pi = 12.891$ kHz).

5. Conclusions

We have demonstrated that studying the R^2 mismatch dependence, $\Delta - \nu_r$, of longitudinal magnetization exchange dynamics in a two-spin system allows extraction of accurate distance information without regard to zero-quantum lineshape parameters. Because the remaining parameters upon which the dynamics depend are easily measured using well-established techniques, we believe this increases the utility of the technique for distance measurements in a wide range of samples. The accompanying information about the zero-quantum lineshape is useful as a measure of the correlation of chemical shift and relaxation at the two sites.

Acknowledgments

Thanks are accorded to C.M. Rienstra and B. Itin for the construction of the probes used in these experiments. This work was supported by grants from the National Institutes of Health (GM-23403 and RR-00995).

References

[1] G.M. Clore, A.M. Gronenborn, Structures of larger proteins in solution: three- and four-dimensional heteronuclear NMR spectroscopy, Science 252 (1991) 1390–1399.
[2] E.R. Andrew, A. Bradbury, R.G. Eades, Nuclear magnetic resonance spectra from a crystal rotated at high speed, Nature 182 (1958) 1659.
[3] I.J. Lowe, Sample rotation in NMR, Phys. Rev. Lett. 2 (1959) 285.
[4] J. Schaefer, E.O. Stejskal, ^{13}C-NMR of polymers spinning at the magic angle, J. Am. Chem. Soc. 98 (1976) 1031–1032.
[5] A.E. Bennett, R.G. Griffin, S. Vega, Recoupling of homo- and heteronuclear dipolar interactions in rotating solids, in: B. Blumich (Ed.), Solid State NMR IV: Methods and Applications of Solid-State NMR, Springer, Berlin, 1994, pp. 1–77.
[6] S. Dusold, A. Sebald, Dipolar recoupling under magic angle spinning conditions, Ann. Rep. NMR Spectrosc. 41 (2000) 185–264.
[7] D.P. Raleigh, M.H. Levitt, R.G. Griffin, Rotational resonance in solid state NMR, Chem. Phys. Lett. 146 (1988) 71–76.
[8] M.H. Levitt, D.P. Raleigh, F. Creuzet, R.G. Griffin, Theory and simulations of homonuclear spin pair systems in rotating solids, J. Chem. Phys. 92 (11) (1990) 6347–6364.
[9] F. Creuzet, A.E. McDermott, R. Gebhard, K. van der Hoef, M.B. Spijker-Assink, J. Herzfeld, J. Lugtenburg, M.H. Levitt, R.G. Griffin, Determination of membrane protein structure by rotational resonance NMR: bacteriorhodopsin, Science 251 (4995) (1991) 783–786.
[10] J.M. Griffiths, T.T. Ashburn, M. Auger, P.R. Costa, R.G. Griffin, P.T. Lansbury Jr., Rotational resonance solid-state NMR elucidates a structural model of pancreatic amyloid, J. Am. Chem. Soc. 117 (1995) 3539–3546.
[11] P.T. Lansbury Jr. et al., Stuctural model for the β amyloid fibril: interstrand alignment of an antiparallel β sheet comprising a C-terminal peptide, Nat. Struct. Biol. 2 (1995) 990–998.
[12] X. Feng et al., Direct determination of a molecular torsion angle in the membrane protein rhodopsin by solid-state NMR, J. Am. Chem. Soc. 119 (1997) 6853–6857.
[13] J. Heller, R. Larsen, M. Ernst, A.C. Kolbert, M. Baldwin, S.B. Prusiner, D.E. Wemmer, A. Pines, Application of rotational resonance to inhomogeneously broadened systems, Chem. Phys. Lett. 251 (3–4) (1996) 223–229.
[14] A. Pines, M.G. Gibby, J.S. Waugh, Proton-enhanced NMR of dilute spins in solids, J. Chem. Phys. 59 (1973) 569–590.
[15] N.C. Nielsen, H. Bildsøe, H.J. Jakobsen, M.H. Levitt, Double-quantum homonuclear rotary resonance: efficient dipolar recovery in magic-angle spinning nuclear magnetic resonance, J. Chem. Phys. 101 (3) (1994) 1805–1812.
[16] K. Halverson, Ph.D. Thesis, MIT, 1991.
[17] P.R. Costa, B.Q. Sun, R.G. Griffin, Rotational resonance tickling: accurate internuclear distance measurement in solids, J. Am. Chem. Soc. 119 (44) (1997) 10821–10830.
[18] E.L. Hahn, Spin echoes, Phys. Rev. 80 (1950) 580.
[19] Z.H. Gan, D.M. Grant, Rotational resonance in a spin-lock field for solid-state NMR, Chem. Phys. Lett. 168 (3–4) (1990) 304–308.
[20] A. Wokaun, R.R. Ernst, Selective detection of multiple quantum transitions in NMR by 2-dimensional spectroscopy, Chem. Phys. Lett. 52 (3) (1977) 407–412.
[21] S. Vega, Fictitious spin-1/2 operator formalism for multiple quantum NMR, J. Chem. Phys. 68 (12) (1978) 5518–5527.
[22] M.H. Levitt, T.G. Oas, R.G. Griffin, Rotary resonance recoupling in heteronuclear spin pair systems, Isr. J. Chem. 28 (4) (1988) 271–282.
[23] A. Kubo, C.A. McDowell, Spectral spin diffusion in polycrystl-aline solids under magic-angle spinning, J. Chem. Soc., Faraday Trans. 1 84 (11) (1988) 3713–3730.
[24] D.L. Van der Hart, G.C. Campbell, Off-resonance proton decoupling on-resonance and near-resonance, J. Magn. Reson 134 (1998) 88–112.
[25] P.J. Carroll, P.L. Stewart, S.J. Opella, Structures of 2 model peptides-*N*-acetyl-D,L-valine and *N*-acetyl-L-valyl-L-leucine, Acta Crystallogr. 46 (1990) 243–246.
[26] J.J. Verbist, M.S. Lehmann, T.F. Koetzle, W.C. Hamilton, Neutron diffraction determination of the structure of Gly–Gly–HCl–H_2O, Acta Crystallogr. B 28 (1972) 3006.
[27] A.E. Bennett, C.M. Rienstra, J.M. Griffiths, W. Zhen, P.T. Lansbury Jr., R.G. Griffin, Homonuclear radio frequency-driven recoupling in rotating solids, J. Chem. Phys. 108 (1998) 9463–9479.
[28] E.O. Stejskal, J. Schaefer, J.S. Waugh, Magic-angle spinning and polarization transfer in proton- enhanced NMR, J. Magn. Reson. 28 (1) (1977) 105–112.